Journal of Materials Chemistry A

ROYAL SOCIETY OF CHEMISTRY

PAPER

View Article Online
View Journal | View Issue

Cite this: J. Mater. Chem. A, 2024, 12, 26170

A continuous porous porphyrinic polymer thin-film composite membrane for anti-biofouling and molecular sieving†

Jia Xu, *[ab] Hansi Zhang,[a] Xiaolong Ren,[a] Shiyi Yao,[a] Wenhua Fan,[a] Ayman Nafady,[c] Abdullah M. Al-Enizi [c] and Shengqian Ma *[b]

Received 29th June 2024
Accepted 27th August 2024

DOI: 10.1039/d4ta04510f

rsc.li/materials-a

Biofouling has long been a challenging issue for nanofiltration. One practical strategy to address this issue is the development and utilization of novel anti-biofouling membranes. In this contribution, a novel thin-film composite nanofiltration membrane was prepared through the interfacial polymerisation of 5,10,15,20-tetra(4-aminophenyl) porphyrin (TAPP) featuring antibacterial properties under visible light with terephthaloyl chloride (TPC) on a polyacrylonitrile (PAN) ultrafiltration membrane, which was exchanged with deionised water to afford a complete polyamide film. The resultant $TAPP_n$-TPC/PAN membrane displayed high antimicrobial activity under visible light, with an antimicrobial efficiency of 99.3% for *E. coli* and 85.9% for *S. aureus*. Moreover, it exhibited enhanced molecular sieving properties at approximately 400 Da to 600 Da. Furthermore, the membrane was transferable to any substrate, and its area was adjustable. This work suggests a new approach for the large-scale fabrication of novel self-cleaning membranes with anti-biofouling feature for applications in actual water treatments.

1 Introduction

Nanofiltration (NF) membranes, which can be used for the removal of dissolved or suspended solutes with sizes ranging from 1 to 10 nm, have been widely implemented for different wastewater treatments.[1–3] However, the increase in membrane fouling remains a serious problem in NF processes. Membrane fouling encompasses inorganic fouling,[4] organic fouling,[5] and biofouling.[6] In particular, biofouling has been known to contribute more than 45% of all membrane fouling and is a major issue in NF.[7] Biofouling begins with the bacterial adhesion on the membrane surface and then the production of a bio-film containing polysaccharides, other chemical organic substances, and a complex community of microbial cells, which are difficult to remove and eventually induce irreversible damage to the membrane treatment system, demonstrated by the sharp reduction in the membrane flux.[8,9] Developing novel anti-biofouling membranes has been suggested as a practical strategy to control membrane biofouling.

In recent years, the incorporation of biocidal agents into polymeric membranes has emerged as a promising strategy to mitigate biofouling.[10] It has been reported that various inorganic biocidal agents, such as silver ions and nanoparticles,[11] copper ions and nanoparticles,[12] TiO_2,[13] ZnO nanoparticles,[14] and graphene oxide,[15] as well as organic biocidal agents, such as quaternary ammonium compounds,[16] polyzwitterions,[16,17] and guanidine-based compounds,[18] can be incorporated into the polymer membrane matrix to fabricate antibiofouling membranes. Compared to inorganic biocidal agents, organic ones exhibit a good compatibility with membranes and improve their separation performance and lifespan.[19]

A suitable organic material for membrane biofouling reduction is a photosensitiser, which can produce singlet oxygen ($^1O_2$) under visible light that can inhibit the growth and reproduction of bacteria.[20,21] Porphyrins are promising photosensitiser molecules which could easily be obtained from nature.[22] Furthermore, the chemical synthesis and modification of porphyrins are also well explored and understood.[23–25] Their antibacterial performance is closely associated with their intrinsic antibacterial mechanisation through photodynamic inactivation (PDI).[26] PDI is a process that relies on singlet oxygen, a short-lived and highly oxidative species, which is generated by photosensitisers under visible light irradiation and causes apoptosis.[27] It has been demonstrated that porphyrins can be used for the PDI of microorganisms with a good level of inhibition.[28–30]

Currently, thin-film composite (TFC) membranes, typically composed of an ultrathin and dense polyamide (PA) film and

[a]Key Laboratory of Marine Chemistry Theory and Technology, Ministry of Education, College of Chemistry and Chemical Engineering, Ocean University of China, Qingdao, Shandong, 266100, China. E-mail: qdxujia@sina.com.cn

[b]Department of Chemistry, University of North Texas, 1508 W Mulberry St, Denton, TX, 76201, USA. E-mail: Shengqian.Ma@unt.edu

[c]Department of Chemistry, College of Science, King Saud University, Riyadh 11451, Saudi Arabia

† Electronic supplementary information (ESI) available. See DOI: https://doi.org/10.1039/d4ta04510f

a porous ultrafiltration (UF) substrate, are dominating the market for NF membranes.[31] In comparison with the conventional single-layer NF membranes, TFC membranes, which are fabricated *via* interfacial polymerisation (IP), exhibit higher permeability and selectivity.[4,5] From the view of antibacterial design, antibacterial nanomaterials could be used as monomers and be reacted with another phase of monomers to form an antibacterial PA film.[18] It has been reported that 5,10,15,20-tetra(4-aminophenyl)porphyrin (TAPP), with four amino groups, could be co-deposited with aqueous monomers on a substrate, followed by IP with organic monomers to form an antibacterial PA film. As a porphyrin derivative, the antibacterial activity mechanism of TAPP still depends on its photosensitivity. Under visible light conditions, TAPP molecules are excited to higher energy states and generate reactive oxygen species (ROS) with surrounding oxygen molecules, such as singlet oxygen ($^1O_2$). These ROS have strong oxidizing properties and can disrupt the integrity of bacterial cell membranes, leading to leakage of cell contents and cell death.[32] Duong *et al.* prepared hybrid PA films through the IP of TAPP and *m*-phenylene diamine (MPD) mixtures with trimesoyl chloride (TMC).[33] Increasing the porphyrin concentration leads to the production of a smoother and thinner PA film with higher biofouling resistance, which has a low fouling propensity and less water transport resistance. However, the high steric hindrance in TAPP, typically resulting in its poor water-solubility, leads to the production of a discontinuous PA film when TAPP is used alone as the aqueous monomer. Therefore, it is a great challenge to design and fabricate a continuous PA TFC membrane *via* IP with only TAPP as the aqueous monomer.

In this study, a continuous antibacterial NF membrane was successfully fabricated *via* IP. Before IP, a dimethyl sulfoxide/water (DMSO/H_2O) solution was used as the solvent for the aqueous phase to solve the limitation of poor water-solubility of TAPP. Terephthaloyl chloride (TPC) was used as the organic monomer to solve the limitation of the high steric hindrance effect of TAPP, leading to the production of a continuous PA film. After IP, the aqueous solution was exchanged with deionised (DI) water to obtain the complete PA layer. These fabricated membranes exhibited elevated antimicrobial activity under visible light and suitable cut-off efficiency. Meanwhile, the membranes were transferable to any substrate, and their areas were adjustable. The effects of TAPP on the membrane morphology and the chemical composition of the PA layer were comprehensively investigated. Separation performance and antibacterial efficiency were also evaluated.

2 Experimental

2.1. Materials

Unless stated otherwise, all solutions and reagents were used without further purification. TPC (>99%) and TAPP (>98%), used as the monomers for the IP of the NF membranes, were purchased from Sigma-Aldrich and Jilin Province Yanshen Technology (China), respectively. TMC (>98%) and MPD (>99%), used as the monomers for IP of the reverse osmosis membranes, were purchased from Sigma-Aldrich. The PAN UF membrane (molecular weight cut off MWCO = 40 kDa), used as the substrate, was supplied by Xiamen Guochu Technology. *Escherichia coli* (*E. coli*) and *Staphylococcus aureus* (*S. aureus*), used as the test bacteria, were purchased from Shanghai Luwei Microbial Science and Technology Co., Ltd. Nutrient broth and nutrient agar were provided by Beijing Land Bridge Technology Co., Ltd. Triethylamine, *n*-hexane (≥97%), NaCl (≥99%), and DMSO (≥99%) were purchased from Shanghai Sinopharm Chemical Reagent Co., Ltd. Rose Bengal (RB), Brilliant Blue R, Acid Lorraine, Chromotrope 2R, Chromotrope FB and Methylene Blue dyes (>95%) were purchased from Sigma-Aldrich. DI water, with a resistivity of 18.0 MΩ cm, was prepared using a Millipore Milli-Q water purification system.

2.2. Membrane preparation

To improve the solubility of TAPP, a DMSO/H_2O solution was selected as the solvent for the preparation of the aqueous solution. However, the nucleophilic addition reaction of acyl chloride with DMSO affects the structure of the PA layer. Therefore, it is necessary to study the effect of DMSO on the separation performance of the PA film. The most commonly used aqueous and organic-phase monomers in forming PA separation layers are MPD and TMC. Therefore, by exploring the effect of DMSO on MPD-TMC PA separation layers, the optimal amount of DMSO to be used in the experiments was determined. MPD was dissolved in different concentrations of DMSO solutions to prepare a 2.0 wt% aqueous solution. Self-standing thin PA films were fabricated by pouring the TMC solution in hexane into the MPD solution in DMSO/H_2O. IP was performed at 25 °C for 1 min. Subsequently, the film was transferred onto a PAN substrate and air-dried overnight. Each PA membrane was labelled as the PA/DMSO$_m$ membrane, where m represents the DMSO concentration.

NF membranes with TAPP as the aqueous monomer were fabricated *via* IP, which was carried out in a silica container. In detail, a certain amount of TAPP was dissolved in DMSO and then mixed with DI water to prepare the aqueous solution. Subsequently, the aqueous solution was poured into a silica container, and the TMC/*n*-hexane solution (0.1 wt%) was poured onto the surface of the aqueous for 5 min to conduct IP. Thereafter, the organic solution was transferred into a separate container, and the top of the PA layer was washed 3 times with fresh *n*-hexane. Afterward, the aqueous phase was transferred into a separate container, and the bottom of the PA film was washed 3 times with DI water to remove the DMSO. Finally, the PA film was dropped onto a silica wafer and then transferred into a big container. It could be floated on the surface of water and be transferred onto a PAN substrate, and then it was air dried overnight. Each NF membrane was labelled as the TAPP$_n$-TPC/PAN membrane, where n represents the mass (mg) of TAPP in 100 g of the aqueous phase solution.

2.3. Membrane characterization

The morphology of the TAPP$_n$-TPC/PAN membranes was examined using a scanning electron microscope (SEM) (Hitachi, S-4800, Japan) with an accelerating voltage of 10 kV. The

chemical composition of the membrane was observed using a Fourier-transform infrared (FTIR) spectrometer (Tensor27, Bruker, Germany) in attenuated total reflection mode with a resolution of 4 cm^{-1}, and the spectrum was collected from 400 to 4000 cm^{-1}. Surface hydrophilicity was evaluated through water contact angle measurements using a contact angle goniometer (Kruss, DSA100, Germany). The elemental composition of the membrane surface was studied using X-ray photoelectron spectroscopy (XPS) (Escalab 250Xi, Thermo Fisher Scientific, America).

2.4. Separation performance evaluation

The membranes were mounted into a dead-end filtration system with an effective membrane area of 11.34 cm^2. The measurements were conducted at room temperature and a trans-membrane pressure drop of 2 bar. The water flux (J_w) and water permeance (P) were calculated using eqn (1):

$$J_W = \frac{V}{A \times t} \quad (1)$$

$$P = \frac{J_W}{\Delta P} \quad (2)$$

where J_w is the pure water flux (L m^{-2} h^{-1}), V is the permeate volume (L), A is the effective membrane area (m^2), Δt is the time of filtraiton (h), P is permeance (L m^{-2} h^{-1} bar^{-1}) and Δp is the trans-membrane pressure drop (bar).

The feed concentration of the dye solutions is 20 ppm. The concentration of dye in the testing solutions was calculated from the absorption values at its characteristic wavelength, respectively. To exclude the effect of solute adsorption, the concentrations of the feed solution and permeate solution were analyzed when the permeation reached a steady state. All permeation processes are repeated at least three times and the average values are reported, and each sample was tested continuously for three cycles. The rejection (R) of the dyes was calculated using eqn (3).

$$R = \left(\frac{C_F - C_P}{C_F}\right) \times 100\% \quad (3)$$

where R is the dye rejection (%), C_F is the concentration of the feed solutions, and C_P is the concentration of the permeate solutions.

2.5. Anti-microbial activity

The antimicrobial activity was evaluated using the colony counting method,[34] and *E. coli* and *S. aureus* were used as the model microorganisms. Prior to the evaluation, all supplies used in the antibacterial experiment were disinfected at 120 °C for 20 min, and the clean bench was put under an ultraviolet lamp for 24 h. The bacteria (*E. coli* and *S. aureus*) were first cultured in a Luria–Bertani (LB) liquid culture medium at 37 °C for 24 h in an incubator shaker, and then the solutions were diluted to a predetermined concentration using the standard serial dilution method. All membrane samples were cut into small pieces (1 cm × 2 cm) and then sterilised with the glassware under ultraviolet radiation for 30 min. Afterward, the membrane samples were put into separate cuvettes containing 10 mL of the bacteria suspension and divided into two groups: one was exposed to visible light for 30 min, and the other was placed in the dark for 30 min. Finally, the cuvettes with the membranes continuously shaken at 37 °C for 24 h, and 100 μL of the dilute solution in the cuvettes were spread onto an LB solid culture medium, followed by dilution 10 times and incubation in an incubator for 24 h. The numbers of colonies on the culture dish were counted using the plate count method. For the blank control, a bacterial suspension with no membrane sample for culturing was subjected to the same conditions. To minimise the experimental error, each sample was tested three times. The antibacterial efficiency (E_b) was obtained using eqn (4).

$$E_b = \frac{(B - C)}{B} \times 100\% \quad (4)$$

where B is the number of blank colonies, and C is the number of colonies of membranes.

3 Results and discussion

The fabrication of the TAPP$_n$-TPC/PAN membrane, as well as its structure and antibacterial function, are presented in Scheme 1. As shown in Scheme 1, there are three crucial strategies for obtaining a continuous membrane: (1) using DMSO/H_2O solvent because of the good solubility of TAPP in DMSO; (2) using TPC as the organic monomer to reduce the high steric hindrance effect of TAPP; and (3) exchanging the aqueous solution with DI water to prevent the membrane breakage caused by the difference in the surface tension between the aqueous solution on the bottom of the PA film and the water in the big container.

3.1. Effect of DMSO on the separation performance of the PA/DMSO$_m$ membrane

Generally, water and *n*-hexane are used as the solvents of the aqueous phase and the organic phase, respectively, for IP. However, TAPP is insoluble in both water and *n*-hexane. Therefore, it is important to determine and employ a solvent that can completely dissolve TAPP. Among the organic solvents miscible with water, DMSO is a suitable solvent for TAPP, and thus a DMSO/H_2O solution was selected as the solvent for the aqueous phase. Due to the possible nucleophilic addition reaction between DMSO and TMC, it was necessary to investigate the effect of DMSO on the PA film and its separation performance to optimise the DMSO dosage. The results are shown in Fig. 1. As the concentration of DMSO increased from 0 to 60 wt%, the water permeance continuously increased from 1.2 to 2.9 L m^{-2} h^{-1} bar^{-1}, while NaCl rejection gradually deteriorated from 95.0% to 94.3% (Fig. 1a). This could be attributed to the nucleophilic addition reaction between DMSO and TMC, which limits the IP reaction between TMC and MPD. It is possible that the degree of cross-linking of the PA layer decreased, which led to the increase in pure water flux and the decrease in NaCl rejection. Compared to the PA membrane without DMSO, the membranes containing DMSO exhibited

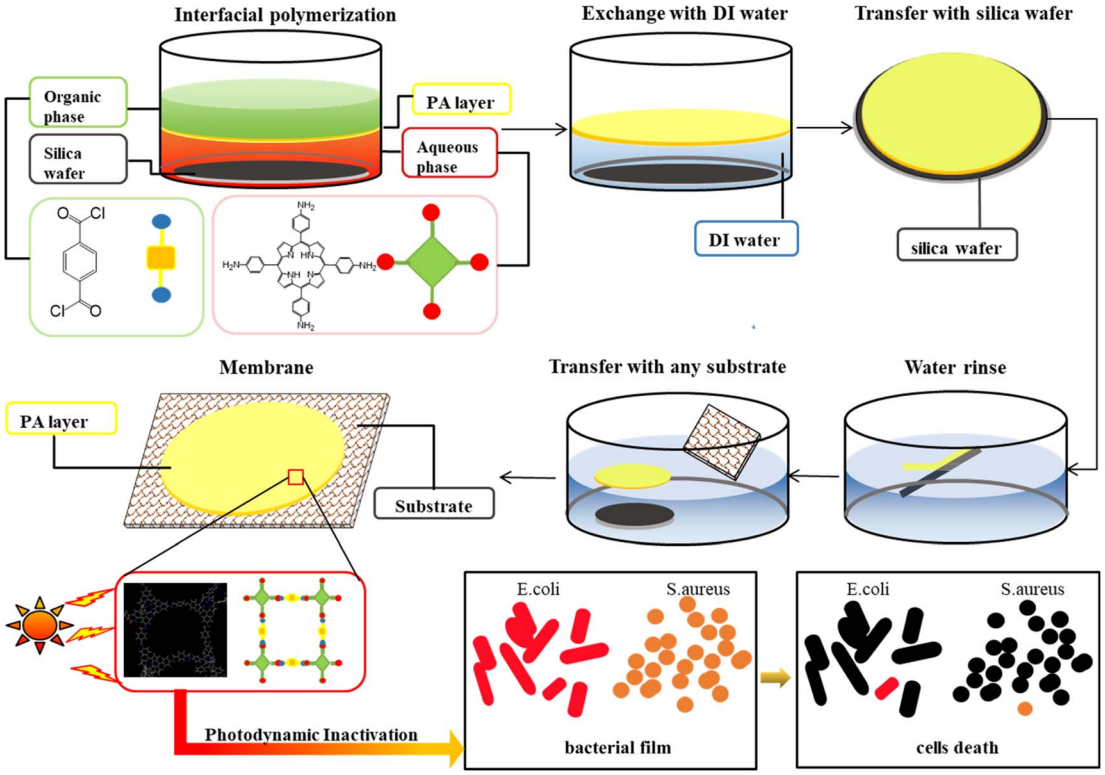

Scheme 1 Illustration of fabrication, structure and antibacterial function of TAPP$_n$/TPC-PAN membranes.

a looser surface with a more crumpled structure (Fig. 1b–g), and the crumples on the membrane surface increased as the DMSO content increased. As previously reported,[35] PA films with an extensively crumpled surface morphology have a higher specific surface area, leading to their increased water permeance. Based on both the satisfactory pure water flux and NaCl rejection, the concentration of DMSO was fixed at 50 wt% for the subsequent experiments.

The TAPP dissolved in the solvent was used to prepare the PA/TAPP$_n$-TPC layer. It was expected to prepare a self-standing PA/TAPP$_n$-TPC layer that can be continuous on the water surface. However, when the highly rigid PA/TAPP$_n$-TPC layer was transferred onto the water surface through the silica wafer, it rapidly broke due to the difference in the surface tension between the water and the remaining aqueous phase on the bottom of the PA/TAPP$_n$-TPC layer (Fig. 2a). Another continuous self-standing PA/TAPP$_n$-TPC layer was prepared with an additional step of exchanging the aqueous phase with DI water before transferring the PA/TAPP$_n$-TPC layer to the water surface, which eliminates the effect of the differences in the surface tension. Finally, TAPP-TPC$_m$/PAN membranes were fabricated by transferring the PA/TAPP$_n$-TPC layer onto a PAN substrate (Fig. 2a).

The surface morphologies of the membranes were observed under an SEM, as shown in Fig. 2b–e. Compared to the PAN membrane, the TAPP$_{2.4}$-TPC/PAN and TAPP$_{4.0}$-TPC/PAN

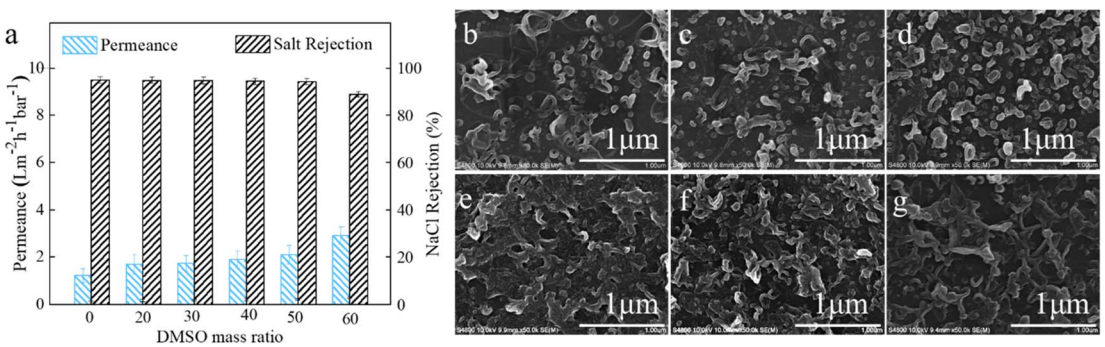

Fig. 1 (a) The influence of DMSO concentration on separation performance; the SEM images of the membrane at concentrations of (b) 0, (c) 20 wt%, (d) 30 wt%, (e) 40 wt%, (f) 50 wt% and (g) 60 wt%.

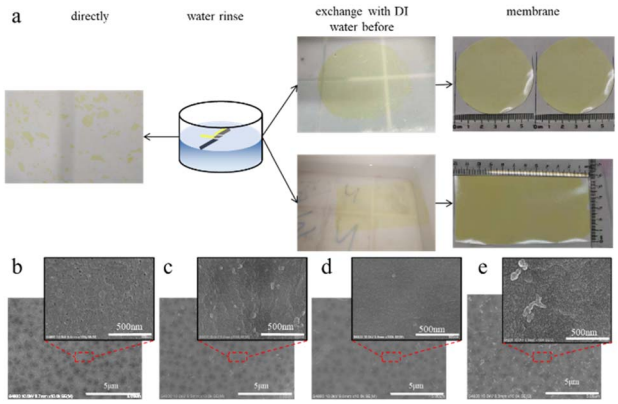

Fig. 2 (a) Different PA/TAPP$_n$-TPC layer; SEM images of (b) PAN, (c) TAPP$_{2.4}$-TPC/PAN, (d) TAPP$_{4.0}$-TPC/PAN and (e) TAPP$_{4.4}$-TPC/PAN membranes.

membranes exhibited a continuous surface with more pea structures (Fig. 2b–d), and the number of peas on the membrane surface decreased as the TAPP content increased (Fig. 2b–d). Pea structures were also observed on the TAPP$_{4.4}$-TPC/PAN membrane, but they were bigger than those found in the other samples. Excess TAPP tends to aggregate, which decreases the degree of cross-linking of TAPP and TPC, leading to a decrease in dye rejection and water permeance. A PA layer with a surface morphology of extensive pea structures could yield a higher specific surface area, leading to a higher water permeance. The surface morphology of the PA layer became denser as the TAPP content increased, which could lead to a higher dye rejection. In future studies, water and dye transport should be observed *via* filtration experiments.

FTIR spectroscopy was used to confirm the chemical composition of the PAN, TAPP$_{2.4}$-TPC/PAN, and TAPP$_{4.0}$-TPC/PAN membranes (Fig. 3a–b). Compared to the PAN membrane, the TAPP$_{2.4}$-TPC/PAN and TAPP$_{4.0}$-TPC/PAN membranes exhibited four distinct peaks at 1270 cm^{-1} (C–N between –NH$_2$ and the benzene ring), 1508 cm^{-1} (C=N on the porphyrin ring), 3015 cm^{-1} (C–H on the pyrrole ring), and 3069 cm^{-1} (N–H in –NH$_2$), which could also be observed in TAPP. Moreover, for the TAPP$_{2.4}$-TPC/PAN and TAPP$_{4.0}$-TPC/PAN membranes, two obvious peaks with similar intensities were observed at 1684 cm^{-1} (stretching vibration of C=O in the amide I band) and 1579 cm^{-1} (combined bending vibration of N–H and stretching vibration of C–N in the amide II band). These are the characteristic absorption peaks of amide (amide I band and amide II band), which are typically found in the spectrum of PA membranes. These results strongly suggest that TAPP$_n$-TPC/PAN membranes were successfully prepared. The hydrophilicity of membranes is an important factor that determines their capability of water transport. To investigate the effect of the concentration of TAPP on the hydrophilicity of the membrane, the water contact angle (WCA) of various membranes was measured, and the results are shown in Fig. 3c.

Compared to the PAN membrane, the TAPP$_n$-TPC/PAN membranes yielded a higher WCA. This indicates that the TAPP$_n$-TPC/PAN membranes are more hydrophobic, and as the TAPP content increased from 0.0028 to 0.0040 wt%, the corresponding WCA increased from 60.1° to 65.8°. Due to the hydrophobicity of TAPP, the hydrophilicity of the TAPP$_n$-TPC/PAN membranes decreased, which could cause water permeability to decline. The zeta potentials of the TAPP$_{2.4}$-TPC/PAN and TAPP$_{4.0}$-TPC/PAN membranes at different pH levels are given in Fig. 3d. The results showed that the membranes were negatively charged, mainly because of the existing carboxyl groups caused by incomplete acid chloride hydrolysis. The TAPP$_{2.4}$-TPC/PAN membranes exhibited a more negative zeta potential, owing to the unreacted acid chloride groups, which may lead to a lower degree of cross-linking.

To characterise and analyze the chemical structure of the PA films, three elements, C, O, and N, were detected on the top layer of the TAPP$_{2.4}$-TPC/PAN and TAPP$_{4.0}$-TPC/PAN membranes *via* XPS, as shown in Fig. 4. The C1s XPS spectra of the TFC membranes were used to analyse the C species on the membrane surface. Fig. 4a–b indicate three kinds of C species existing in the membrane surface, corresponding to the binding energies of 284.8 eV (C–C/C–H), 286.5 eV (C–N), and 288 eV (C=O). The C=O/C–N atomic ratios of the fabricated skin layer were calculated, which indirectly determined the degree of network cross-linking of the PA layers. The atomic ratios of C=O/C–N of the PA skin layers decreased from 0.5 to 0.2 as the TAPP concentration increased from 0.0024 wt% min to 0.0040 wt%, indicating the low degree of cross-linking of the PA skin layer at the TAPP concentration of 0.0024 wt%. The deconvoluted N1s and O1s XPS spectra of these were also obtained. The spectra indicate the existence of five N species, corresponding to the binding energies of 397.7 eV (C–N=C), 398.7 eV (C–NH$_2$), 399.8 eV (C–NH–C), 400.4 eV (N–C=O) and 401.7 eV (C–N$^+$H$_3$), and two kinds of oxygen species, with the binding energies of 532.4 eV (O=C–O) and 531.4 eV (O=C–N).

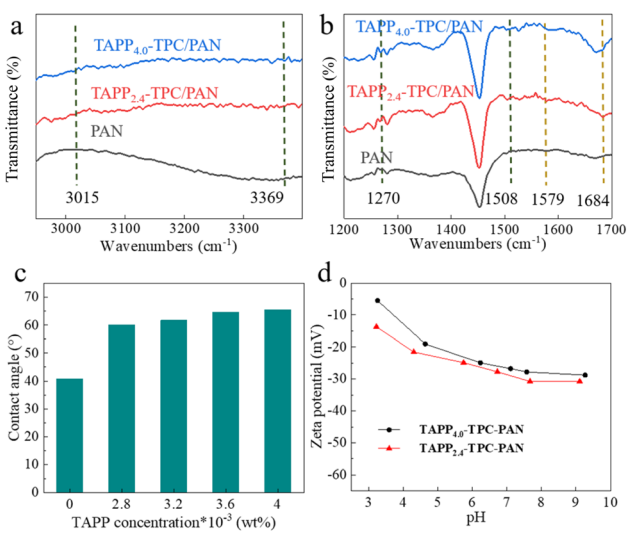

Fig. 3 FTIR images of PAN, TAPP$_{2.4}$-TPC/PAN and TAPP$_{4.0}$-TPC/PAN membranes at different wavenumber scales (a) 2950–3390 cm^{-1}, (b) 1200–1700 cm^{-1}; (c) water contact angle of various membranes; (d) zeta potentials of various membranes.

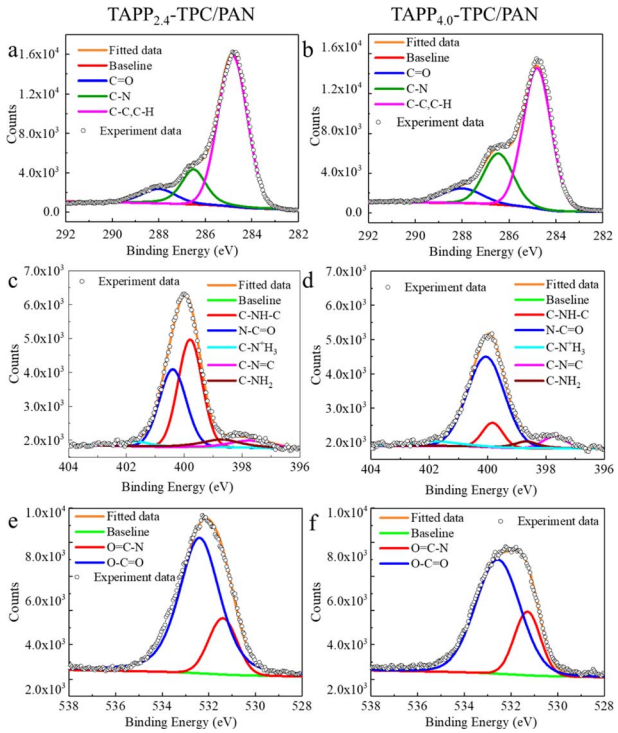

Fig. 4 XPS core level spectra of $TAPP_{2.4}$-TPC/PAN and $TAPP_{4.0}$-TPC/PAN membranes. (a and b) Convoluted high resolution C1s, (c and d) convoluted high resolution N1s and (e and f) convoluted high resolution O1s for (a, c and e) $TAPP_{2.4}$-TPC/PAN and (b, d and f) $TAPP_{4.0}$-TPC/PAN membranes.

3.2. Separation performance of $TAPP_n$-TPC/PAN membranes

Permeation tests with 20 ppm of RB dye solution were performed to investigate the water permeance and separation performance of the $TAPP_n$-TPC/PAN membranes. The results are shown in Fig. 5a. The water permeance of the $TAPP_n$-TPC/PAN membranes significantly decreased as the TAPP concentration increased. Denser surfaces slow down water penetration; therefore, the decrease in the water permeance of the membranes was probably due to the denser membrane surface with fewer pea structures (Fig. 2b–d). The contrary trend was found for water flux during the RB/H_2O filtration test at the TAPP concentrations from 0.0024 wt% to 0.0040 wt%. The RB dye rejection of the $TAPP_n$-TPC/PAN membranes reached a maximum at the TAPP concentration of 0.0040 wt% and then decreased at the concentration of 0.0044 wt%. Excess TAPP tends to aggregate, which decreases the degree of cross-linking of TAPP and TPC, leading to a decrease in the dye rejection (Fig. 2e). Thus, the $TAPP_{4.0}$-TPC/PAN membrane was chosen for the selective dye molecular sieving experiment. The rejection of dyes (20 ppm) with different molecular weights in water is plotted in Fig. 5b. All dyes showed a consistent S-shaped rejection curve with molecular weight, which is important for selective dye molecular sieving. The membrane exhibited a sharp molecular sieving with an MWCO value of approximately 600 Da and molecular weight retention onset at around 400 Da. As shown in Table S4,† compared to the reported literature on the rejection performance of membranes for dyes with different molecular weights, the nanofiltration membrane prepared in this work can achieve selective rejection or purification of dyes with specific molecular weights.[36–40]

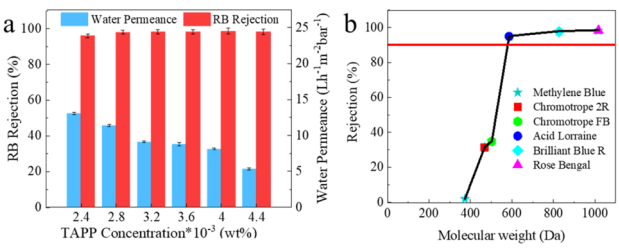

Fig. 5 Permeability and separation performance of $TAPP_n$-TPC/PAN membranes. (a) Water permeance and RB rejection of $TAPP_n$-TPC/PAN at different TAPP concentrations; (b) rejection of dyes with different molecular weights of the $TAPP_{4.0}$-TPC/PAN membrane.

3.3. Versatile antimicrobial properties of membranes

In this study, Gram-negative *E. coli* and Gram-positive *S. aureus* were used as the model bacteria to evaluate the antimicrobial activity of the membrane. Fig. 6 shows the bacteria colonies on the nutrient agar plates for the blank control (without the membrane), PAN, $TAPP_{2.4}$-TPC/PAN, and $TAPP_{4.0}$-TPC/PAN membranes in the dark and under visible light. Prior to the antimicrobial property test, the PDI of TAPP was investigated. As shown in Fig. 6, compared to the blank control, TAPP shows versatile (Gram-negative *E. coli* and Gram-positive *S. aureus*) antibacterial activity, and the inhibition rate of TAPP under visible light is higher than that in the dark, which indicates that TAPP has good PDI properties and is suitable for use in antibiofouling membranes. After that, the antimicrobial properties of membranes were investigated. It is clearly seen that the $TAPP_n$-TPC/PAN membranes have better antibacterial activity in the dark and under visible light than the PAN membrane, which indicates that the toxicity of the PA/$TAPP_n$-TPC layer is the principal reason for the observed reduction in the number of

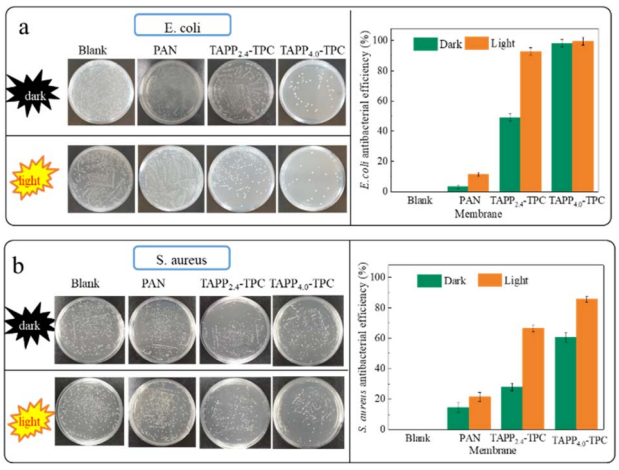

Fig. 6 *E. coli* and *S. aureus* colonies on the nutrient agar plates and antibacterial efficiency (E_b) for blank control (without the membrane), PAN, $TAPP_{2.4}$-TPC/PAN, and $TAPP_{4.0}$-TPC/PAN membranes in the dark and under visible light, respectively. (a) *E. coli* and (b) *S. aureus*.

live bacteria. In contrast to the biofilm growth in the dark, the formation of biofilms under irradiation with 460 nm light was quite inhibited due to the PDI of the PA/TAPP$_n$-TPC layer. The TAPP$_{2.4}$-TPC/PAN and TAPP$_{4.0}$-TPC/PAN membranes exhibited excellent PDI for both *E. coli* and *S. aureus*.

Based on the results of colony forming-count method (Fig. 6), there was a considerable reduction in the number of *E. coli* with the antibacterial efficiency (E_b) of 92.6% and 99.3% for TAPP$_{2.4}$-TPC/PAN and TAPP$_{4.0}$-TPC/PAN membranes, respectively, and in the number of *S. aureus* with the E_b of 66.3% and 85.9% for TAPP$_{2.4}$-TPC/PAN and TAPP$_{4.0}$-TPC/PAN membranes, respectively, relative to the blank control (without the membrane). This indicates that a small quantity of TAPP, used as a monomer in the fabrication of NF membranes, can significantly decrease the number of viable bacterial cells. Compared with published literature, Table S5† further demonstrates that the fabricated NF membranes using TAPP as a monomer have better antibacterial performance, especially for *E. coli*.[41–46]

3.4. Membrane stability and strategy generality

Scaling up is another key step for the practical implementation of membranes. In this work, we successfully scaled up our PAN-supported membrane in terms of area, from 28 to 63 cm^2 (Fig. 2a). The membrane with a large area (63 cm^2) exhibited promising NF performance, with a dye rejection of 98.4%. Furthermore, the PA layer could be transferred to other surfaces for bacterial inhibition.

4 Conclusions

In conclusion, we fabricated a polyamine-based nanofiltration (TAPP$_n$-TPC/PAN) membrane with excellent antimicrobial capability and high separation efficiency *via* interfacial polymerization. The continuous membrane was realized *via* three strategies of "mixing solvent", "paraphthaloyl chloride (TPC) as an organic monomer" and "exchanging aqueous solution with DI water", solving the issues of poor solubility, high steric hindrance effect of TAPP and difference in surface tension. The TAPP$_n$-TPC/PAN membranes possess a smoother and denser surface and their hydrophilicity decreases with a higher TAPP concentration. The resulting TAPP$_{4.0}$-TPC/PAN membranes exhibited a better separation performance (RB rejection of 99.5%) and exhibited enhanced molecular sieving properties with approximately 400 Da to 600 Da. Meanwhile, an excellent anti-biofouling performance with an anti-bacterial efficiency of 99.3% for *E. coli* and 85.9% for *S. aureus* under visible light were achieved. Moreover, the PA layer could be transferred to other surfaces and scaled-up. The membrane fabrication technique in this work offers significant opportunities to exploit the unique properties of photosensitizers in the fabrication of various separation membranes.

Data availability

The data that support the findings of this study are available from the corresponding author upon reasonable request. This includes raw and processed data generated during the current study. Any additional data or materials required for replication of the results can also be provided by the corresponding author.

Conflicts of interest

There are no conflicts to declare.

Acknowledgements

This work was supported by the National Natural Science Foundation of China (No. 22378374). Partial support from the Robert A. Welch Foundation (B-0027) (S. M.) and Researchers Supporting Program (No. RSP-2024R55) (A. N.) at King Saud University, Riyadh, Saudi Arabia is also acknowledged.

Notes and references

1 W. J. Lau, S. Gray, T. Matsuura, D. Emadzadeh, J. P. Chen and A. F. Ismail, *Water Res.*, 2015, **80**, 306–324.
2 A. W. Mohammad, Y. H. Teow, W. L. Ang, Y. T. Chung, D. L. Oatley-Radcliffe and N. Hilal, *Desalination*, 2015, **356**, 226–254.
3 K. Y. Wang and T.-S. Chung, *J. Membr. Sci.*, 2006, **281**, 307–315.
4 D. Lin, Z. Yan, X. Tang, J. Wang, H. Liang and G. Li, *Sci. Total Environ.*, 2019, **670**, 685–695.
5 K. Chon, S. Sarp, S. Lee, J.-H. Lee, J. A. Lopez-Ramirez and J. Cho, *Desalination*, 2011, **272**, 128–134.
6 Y. Yang, C. Li and L.-A. Hou, *Environ. Sci. Pollut. Res.*, 2019, **26**, 30575–30583.
7 S. Beisl, S. Monteiro, R. Santos, A. S. Figueiredo, M. Guadalupe Sanchez-Loredo, M. A. Lemos, F. Lemos, M. Minhalma and M. N. de Pinho, *Water Res.*, 2019, **149**, 225–231.
8 D. Y. Koseoglu-Imer, B. Kose, M. Altinbas and I. Koyuncu, *J. Membr. Sci.*, 2013, **428**, 620–628.
9 J.-H. Li, X.-S. Shao, Q. Zhou, M.-Z. Li and Q.-Q. Zhang, *Appl. Surf. Sci.*, 2013, **265**, 663–670.
10 J. Zhu, J. Hou, Y. Zhang, M. Tian, T. He, J. Liu and V. Chen, *J. Membr. Sci.*, 2018, **550**, 173–197.
11 S. Liu, F. Fang, J. Wu and K. Zhang, *Desalination*, 2015, **375**, 121–128.
12 M. Khajouei, M. Jahanshahi and M. Peyravi, *J. Taiwan Inst. Chem. Eng.*, 2018, **85**, 237–247.
13 V. Kochkodan, S. Tsarenko, N. Potapchenko, V. Kosinova and V. Goncharuk, *Desalination*, 2008, **220**, 380–385.
14 X. Huang, Y. Chen, X. Feng, X. Hu, Y. Zhang and L. Liu, *J. Membr. Sci.*, 2020, **602**, 117956.
15 H. Li, H. Zhang, X. Qin and W. Shi, *Appl. Surf. Sci.*, 2017, **407**, 260–275.
16 H. Peng, Q. Tang, S. Tang, J. Gong and Q. Zhao, *J. Membr. Sci.*, 2019, **592**, 117386.
17 Y.-F. Mi, Q. Zhao, Y.-L. Ji, Q.-F. An and C.-J. Gao, *J. Membr. Sci.*, 2015, **490**, 311–320.
18 X. Li, Y. Cao, H. Yu, G. Kang, X. Jie, Z. Liu and Q. Yuan, *J. Membr. Sci.*, 2014, **466**, 82–91.

19 Y. Ji, W. Qian, Y. Yu, Q. An, L. Liu, Y. Zhou and C. Gao, *Chin. J. Chem. Eng.*, 2017, **25**, 1639–1652.
20 M. R. Hamblin, *Curr. Opin. Microbiol.*, 2016, **33**, 67–73.
21 Z. Malik, J. Hanania and Y. Nitzan, *J. Photochem. Photobiol., B*, 1990, **5**, 281–293.
22 M. Wainwright, T. Maisch, S. Nonell, K. Plaetzer, A. Almeida, G. P. Tegos and M. R. Hamblin, *Lancet Infect. Dis.*, 2017, **17**, E49–E55.
23 M. Ethirajan, Y. Chen, P. Joshi and R. K. Pandey, *Chem. Soc. Rev.*, 2011, **40**, 340–362.
24 M. Sun, H. Liu, X. Wang, X. Yang, F. Gao, D. Xie, W. Fan, Y. Han, B. Xu and D. Sun, *Chin. J. Struct. Chem.*, 2023, **42**, 100146.
25 X. Wang, M. Xu, W. Fan and D. Sun, *Chin. J. Chem.*, 2023, **41**, 3772–3791.
26 L. Jiang, C. R. R. Gan, J. Gao and X. J. Loh, *Small*, 2016, **12**, 3609–3644.
27 D. Trachootham, J. Alexandre and P. Huang, *Nat. Rev. Drug Discovery*, 2009, **8**, 579–591.
28 J. Hynek, J. Zelenka, J. Rathousky, P. Kubat, T. Ruml, J. Demel and K. Lang, *ACS Appl. Mater. Interfaces*, 2018, **10**, 8527–8535.
29 C. M. B. Carvalho, E. Alves, L. Costa, J. P. C. Tome, M. A. F. Faustino, M. G. P. M. S. Neves, A. C. Tome, J. A. S. Cavaleiro, A. Almeida, A. Cunha, Z. Lin and J. Rocha, *ACS Nano*, 2010, **4**, 7133–7140.
30 A. Tavares, S. R. S. Dias, C. M. B. Carvalho, M. A. F. Faustino, J. P. C. Tome, M. G. P. M. S. Neves, A. C. Tome, J. A. S. Cavaleiro, A. Cunha, N. C. M. Gomes, E. Alves and A. Almeida, *Photochem. Photobiol. Sci.*, 2011, **10**, 1659–1669.
31 M. Paul and S. D. Jons, *Polymer*, 2016, **103**, 417–456.
32 B. M. Amos-Tautua, S. P. Songca and O. S. Oluwafemi, *Molecules*, 2019, **24**, 2456.
33 P. H. H. Duong, P.-Y. Hong, V. Musteata, K. V. Peinemann and S. P. Nunes, *Chemistryselect*, 2017, **2**, 6612–6616.
34 J. Xu, X. Feng, J. Hou, X. Wang, B. Shan, L. Yu and C. Gao, *J. Membr. Sci.*, 2013, **446**, 171–180.
35 Z. Wang, Z. Wang, S. Lin, H. Jin, S. Gao, Y. Zhu and J. Jin, *Nat. Commun.*, 2018, **9**, 2004.
36 E. Maaskant, W. Vogel, T. J. Dingemans and N. E. Benes, *J. Membr. Sci.*, 2018, **567**, 321–328.
37 L. Huang, S. Huang, S. R. Venna and H. Lin, *Environ. Sci. Technol.*, 2018, **52**, 12649–12655.
38 P. Zhang, J.-L. Gong, G.-M. Zeng, B. Song, S. Fang, M. Zhang, H.-Y. Liu, S.-Y. Huan, P. Peng, Q.-Y. Niu, D.-B. Wang and J. Ye, *Sep. Purif. Technol.*, 2019, **220**, 309–319.
39 N. A. Mazlan, A. Lewis, Z. Chen, F. S. Butt, J. Han, N. Radacsi, S. Yang and Y. Huang, *J. Membr. Sci.*, 2024, **697**, 122539.
40 Y. Guo, S. Li, B. Su and B. Mandal, *Chem. Eng. J.*, 2019, **369**, 498–510.
41 S. Dadari, M. Rahimi and S. Zinadini, *Chem. Eng. J.*, 2022, **431**, 134116.
42 Z. Zeng, D. Yu, Z. He, J. Liu, F. X. Xiao, Y. Zhang, R. Wang, D. Bhattacharyya and T. T. Y. Tan, *Sci. Rep.*, 2016, **6**, 20142.
43 X. F. Sun, J. Qin, P. F. Xia, B. B. Guo, C. M. Yang, C. Song and S. G. Wang, *Chem. Eng. J.*, 2015, **281**, 53–59.
44 J. Zhu, J. Wang, A. A. Uliana, M. Tian, Y. Zhang, Y. Zhang, A. Volodin, K. Simoens, S. Yuan and J. Li, *ACS Appl. Mater. Interfaces*, 2017, 28990.
45 H. Chen, F. Zhao, X. Zhang, H.-D. Park, Z. Li and L. Yang, *J. Membr. Sci.*, 2024, **707**, 122992.
46 L. Xu, Z. Pang, H. Yu, M. Guo, X. Yan, X. Jiang and L. Yu, *Desalination*, 2023, **565**, 116809.